



## OPEN ACCESS

## EDITED BY

Chitresh Bhushan,  
GE Global Research, United States

## REVIEWED BY

Haiqing Huang,  
University of Pittsburgh, United States  
Afis Ajala,  
GE Global Research, United States

## \*CORRESPONDENCE

Yoko Ikoma  
ikoma.yoko@qst.go.jp

## SPECIALTY SECTION

This article was submitted to  
Brain Imaging Methods,  
a section of the journal  
Frontiers in Neuroscience

RECEIVED 05 June 2022

ACCEPTED 10 August 2022

PUBLISHED 21 September 2022

## CITATION

Tachibana A, Ikoma Y, Hirano Y,  
Kershaw J and Obata T (2022)  
Separating neuronal activity and  
systemic low-frequency oscillation  
related BOLD responses at nodes of  
the default mode network during  
resting-state fMRI with multiband  
excitation echo-planar imaging.  
*Front. Neurosci.* 16:961686.  
doi: 10.3389/fnins.2022.961686

## COPYRIGHT

© 2022 Tachibana, Ikoma, Hirano,  
Kershaw and Obata. This is an  
open-access article distributed under  
the terms of the [Creative Commons  
Attribution License \(CC BY\)](https://creativecommons.org/licenses/by/4.0/). The use,  
distribution or reproduction in other  
forums is permitted, provided the  
original author(s) and the copyright  
owner(s) are credited and that the  
original publication in this journal is  
cited, in accordance with accepted  
academic practice. No use, distribution  
or reproduction is permitted which  
does not comply with these terms.

# Separating neuronal activity and systemic low-frequency oscillation related BOLD responses at nodes of the default mode network during resting-state fMRI with multiband excitation echo-planar imaging

Atsushi Tachibana<sup>1</sup>, Yoko Ikoma<sup>1\*</sup>, Yoshiyuki Hirano<sup>1,2,3</sup>,  
Jeff Kershaw<sup>1</sup> and Takayuki Obata<sup>1,2</sup>

<sup>1</sup>Department of Molecular Imaging and Theranostics, Institute for Quantum Medical Science, National Institutes for Quantum Science and Technology, Chiba, Japan, <sup>2</sup>Research Center for Child Mental Development, Chiba University, Chiba, Japan, <sup>3</sup>United Graduate School of Child Development, Osaka University, Kanazawa University, Hamamatsu University School of Medicine, Chiba University, and University of Fukui, Suita, Japan

Functional magnetic resonance imaging (fMRI) evaluates brain activity using blood oxygenation level-dependent (BOLD) contrast. Resting-state fMRI (rsfMRI) examines spontaneous brain function using BOLD in the absence of a task, and the default mode network (DMN) has been identified from that. The DMN is a set of nodes within the brain that appear to be active and in communication when the subject is in an awake resting state. In addition to signal changes related to neural activity, it is thought that the BOLD signal may be affected by systemic low-frequency oscillations (SysLFOs) that are non-neuronal in source and likely propagate throughout the brain to arrive at different regions at different times. However, it may be difficult to distinguish between the response due to neuronal activity and the arrival of a SysLFO in specific regions. Conventional single-shot EPI (Conv) acquisition requires a longish repetition time, but faster image acquisition has recently become possible with multiband excitation EPI (MB). In this study, we evaluated the time-lag between nodes of the DMN using both Conv and MB protocols to determine whether it is possible to distinguish between neuronal activity and SysLFO related responses during rsfMRI. While the Conv protocol data suggested that SysLFOs substantially influence the apparent time-lag of neuronal activity, the MB protocol data implied that the effects of SysLFOs

and neuronal activity on the BOLD response may be separated. Using a higher time-resolution acquisition for rsfMRI might help to distinguish neuronal activity induced changes to the BOLD response from those induced by non-neuronal sources.

#### KEYWORDS

resting-state fMRI, default mode network, low-frequency oscillation, multiband EPI, BOLD signal

## Introduction

Brain functional magnetic resonance imaging (fMRI) utilizes blood oxygen level-dependent (BOLD) signal contrast to evaluate the neuronal activity in active areas of the brain (Ogawa et al., 1990). Neuronal activity leads to increased blood flow in specific regions, and the subsequent decrease in deoxy-hemoglobin concentration in the activated region is reflected by an increase in the BOLD signal intensity (Obata et al., 2004; Hirano et al., 2011, 2018). Therefore, the BOLD signal is not a direct measurement of brain activity, but rather a measure of secondary hemodynamic changes triggered by neuronal activation (Buxton et al., 2004; Liu, 2013). In addition to signal changes related to neural activity, the BOLD signal may be affected by global changes in arteriovenous blood flow velocity, cardiac pulsation, and respiration (Chang and Glover, 2009; Chang et al., 2009). Since the effect of those changes on the BOLD response is relatively slow in comparison to neuronal activity-related changes, they are called low-frequency oscillations (LFOs) (Murphy et al., 2013).

Tong et al. (2013) have explored low-frequency contributions to the BOLD signal that they identified as systemic low-frequency oscillations (SysLFOs). SysLFOs are considered to be non-neuronal in source and can be widely observed in the brain using fMRI. Although it is thought that SysLFO signal may derive from Mayer waves, CO<sub>2</sub> concentration fluctuations and vasomotions, the detailed source of the signal is still unclear (Nilsson and Aalkjaer, 2003; Wise et al., 2004; Julien, 2006; Rivadulla et al., 2011; Sassaroli et al., 2012; Golestani et al., 2015). Tong et al. (2013) suggested that SysLFOs are endogenous to the cerebral blood flow and, due to the time they take to propagate, arrive at different regions at different times. Furthermore, if SysLFOs travel throughout the body with the blood flow, it is likely that related signals will be detectable at peripheral sites (Tong and Frederick, 2014). An example of this was provided by a study where near infrared spectroscopy (NIRS) and resting-state fMRI (rsfMRI) were simultaneously performed (Erdoğan et al., 2016). After bandpass filtering the data to the range 0.01–0.1 Hz, it was found that changes in oxygenation measured at the fingertip are significantly correlated with the global BOLD signal (GS),

which was obtained by averaging over the whole brain excluding white matter (WM) and cerebrospinal fluid (CSF). The same group also proposed a method for estimating the arrival time of a SysLFO in a particular region of the brain. The method estimates the delay between the GS and the BOLD signal at each pixel, and then a SysLFO-MAP of the whole brain is created. SysLFO-MAPs were found to have a significant correlation with the cerebral blood flow measured with dynamic susceptibility contrast (DSC) MRI (Erdoğan et al., 2016; Tong et al., 2017).

Resting-state fMRI is performed while the subject is awake and at rest, so the data reflects the idle state of the brain (Biswal, 2012). It is thought that rsfMRI signals demonstrate the mechanical coupling and connectivity between various regions of the brain. One of the most important networks is the default mode network (DMN), which consists of nodes in the posterior cingulate cortex (PCC), left and right lower parietal lobes (L- and R-IPL), and medial prefrontal cortex (mPFC) (Greicius et al., 2003). The connectivity of neuronal activity is considered to be high if the BOLD signal changes at each of these nodes are highly correlated. Various studies have reported an association between brain diseases, such as dementia and schizophrenia, and DMN connectivity (Greicius et al., 2004; Liang et al., 2006; Barkhof et al., 2014).

Assuming there is some delay in the propagation of neuronal activity throughout the brain, it is likely that there is a time-lag between the different nodes of the DMN. However, it may be difficult to distinguish between the time-lag in the response due to neuronal activity and the arrival of a SysLFO in specific regions. The conventional single-shot EPI (Conv) acquisition protocol widely used for rsfMRI takes about 2,000 ms to image the whole brain. In contrast, multiband EPI (MB) acquisition enables imaging of the entire brain in a much shorter time (TR 500 ms), which means that BOLD signals can be measured with improved time-resolution (Feinberg et al., 2010). MB protocol data therefore contains four times more information about separate neuronal and possible SysLFO-related signals than data acquired with a Conv protocol. Using a higher time-resolution acquisition method might help to distinguish neuronal activity related time-lags from SysLFO delays.

In this study, we evaluated the time-lag between nodes of the DMN using both the Conv and MB protocols to determine

whether it is possible to distinguish between neuronal activity and SysLFO related responses during rsfMRI.

## Materials and methods

Eighteen healthy female volunteers (age  $26.6 \pm 7.1$  years) participated in this study. All subjects provided informed consent, and the institutional review board of the National Institutes for Quantum Science and Technology approved the research protocol (# 16-031).

## Data acquisition

All MRI scans were conducted with a clinical 3T MRI system (MAGNETOM Verio 3T; Siemens Healthcare K.K., Erlangen, Germany) equipped with a 32-channel phased-array head matrix coil. A high-resolution T1-weighted sagittal three-dimensional anatomical image was acquired using magnetization prepared rapid-gradient echo (MPRAGE) with the following parameters: TR = 2,300 ms, TE = 1.95 ms, TI = 900 ms, flip angle = 9 degrees, matrix =  $512 \times 512$ , FOV = 250 mm  $\times$  250 mm, slice thickness = 1 mm, total acquisition time = 4 min 33 s. For rsfMRI scanning, Conv protocol data was acquired with the following parameters:

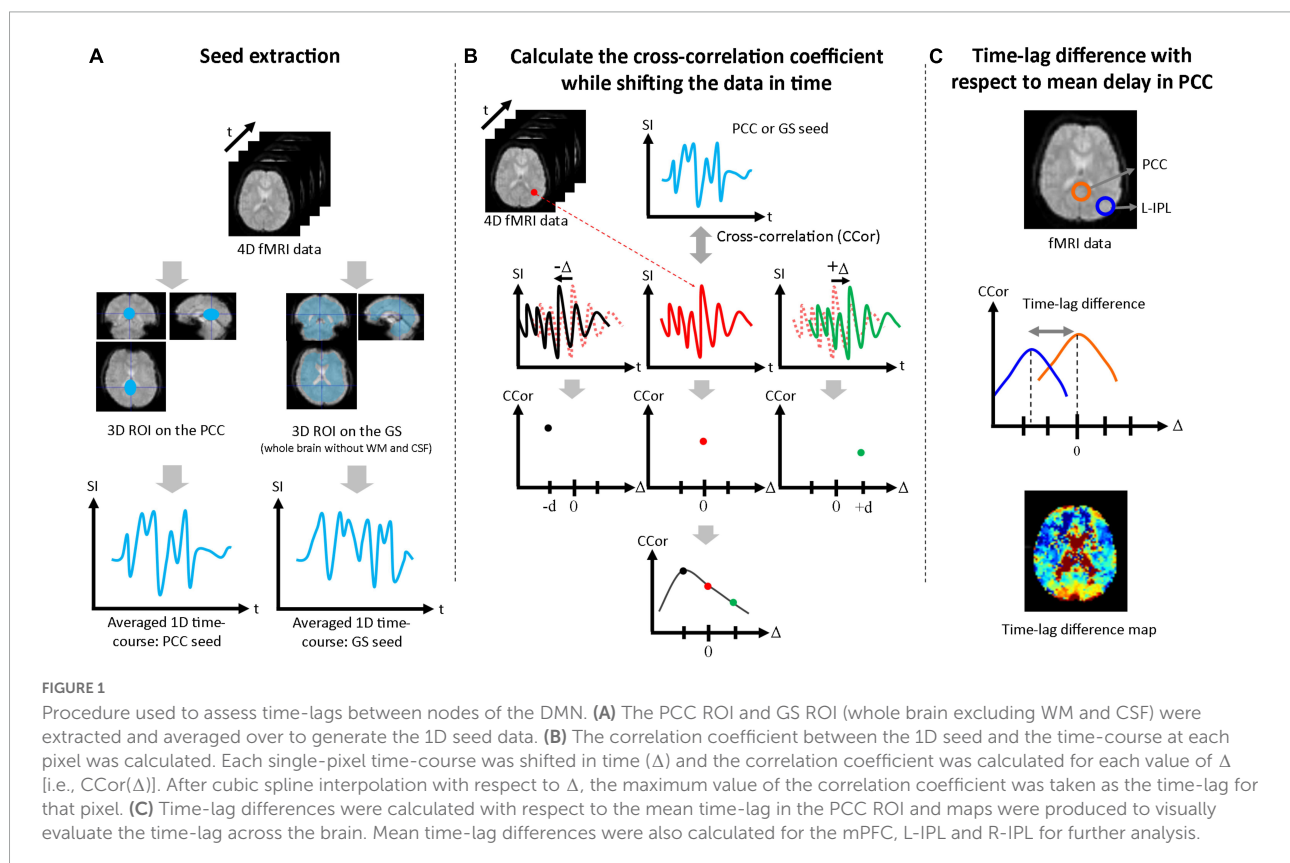
TR = 2,000 ms, TE = 25 ms, flip angle = 90 degrees, matrix =  $64 \times 64$ , FOV = 240 mm  $\times$  240 mm, slice thickness = 3.8 mm, slice gap = 0.5 mm, repetitions = 204, total acquisition time = 6 min 52 s. The high time-resolution MB protocol rsfMRI data was acquired with a multiband EPI sequence (University of Minnesota sequence CMRR MB EPI VD13A R016a) using the following parameters: TR = 500 ms, TE = 30 ms, flip angle = 44 degrees, matrix =  $64 \times 64$ , FOV = 240 mm  $\times$  240 mm, slice thickness = 3.8 mm, slice gap = 0.456 mm, multiband factor = 6, repetitions = 600, total acquisition time = 5 min 7 s. All subjects were instructed to lie still and remain awake with their eyes open while watching a red dot on a screen positioned above them. The datasets generated during the current study are available from the corresponding author on reasonable request.

## Preprocessing

Resting-state fMRI data was preprocessed using DPARSF (Version 4.3<sup>1</sup>) and SPM12.<sup>2</sup> The first 10 images for each subject were discarded to allow the longitudinal magnetization to reach

1 <http://restfmri.net/forum/DPARSF>

2 <https://www.fil.ion.ucl.ac.uk/spm/>

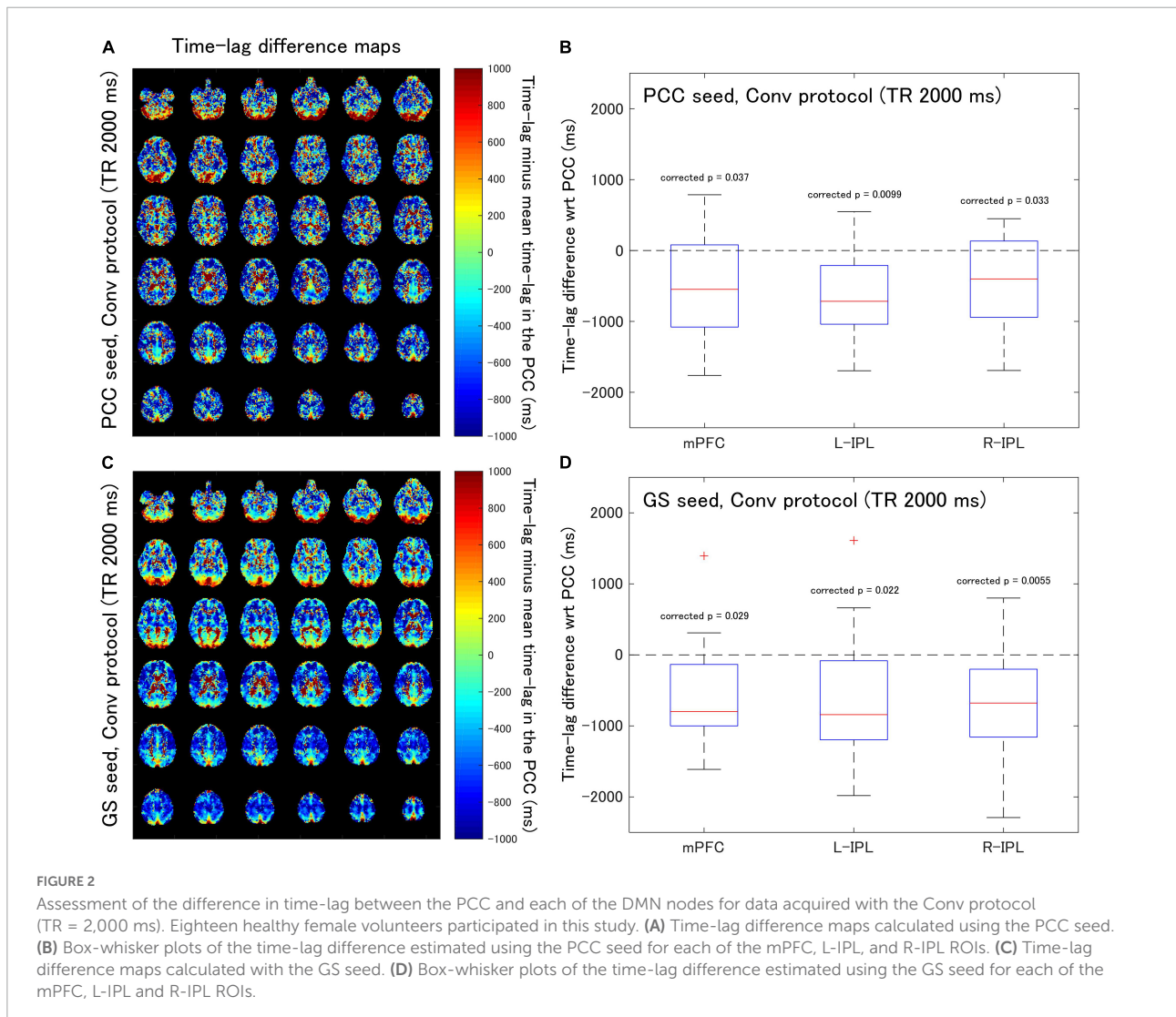


a steady-state. Slice-timing correction and motion correction were both applied. The data was registered and normalized to the Montreal Neurological Institute (MNI) space using the T1 image re-sampled to 3-mm isotropic voxels. Smoothing was performed with a 4 mm FWHM Gaussian kernel. Time courses were filtered for linear trends and then band-pass filtering (0.01–0.1 Hz) was applied. Confounding terms such as head motion, white matter signal and cerebrospinal fluid signal, were regressed out.

## Time-lag analysis

Seed-based correlation analysis was performed to estimate the time-lags due to functional connectivity of the mPFC, L-IPL, and R-IPL with respect to seed data taken from the PCC and GS. First, a three-dimensional volume seed regions of interest (ROI) was drawn for both the PCC and GS (whole brain without WM

and CSF) using the Automated Anatomical Labeling (AAL) brain template, and a one-dimensional seed time-course was produced by averaging over each ROI (Figure 1A). Second, the correlation coefficient was calculated between the one-dimensional seed time-courses and the time-course for each pixel in the brain. The single-pixel time-courses were also shifted in time ( $\Delta$ ), and the correlation coefficient between the seed time-course and the shifted single-pixel time-course at each  $\Delta$  [i.e.,  $CCor(\Delta)$ ] was calculated. The full range of  $\Delta$  was  $\pm 20$  s in 2 s steps for the Conv protocol and  $\pm 5$  s in 0.5 s steps for the MB protocol. Cubic spline interpolation was then applied to  $CCor(\Delta)$  as a function of  $\Delta$  for each pixel, and the  $\Delta$  corresponding to the highest value of  $CCor(\Delta)$  was defined to be the time-lag for that pixel (Figure 1B). To facilitate comparison between the PCC and GS seed results, the mean time-lag in the PCC ROI was calculated and then subtracted from the time-lag of each pixel. Time-lag difference maps were then produced to visually evaluate the time-lag across the brain (Figure 1C),





and the mean values in the mPFC, L-IPL, and R-IPL were calculated using ROIs drawn with reference to the AAL brain template. The Wilcoxon signed-rank test was then performed to determine whether the time-lags of each of the DMN nodes with respect to the PCC were significantly different from zero. Bonferroni correction for multiple comparisons was performed by multiplying each  $p$ -value by 3 for the three different nodes of the DMN.

## Correlation analysis

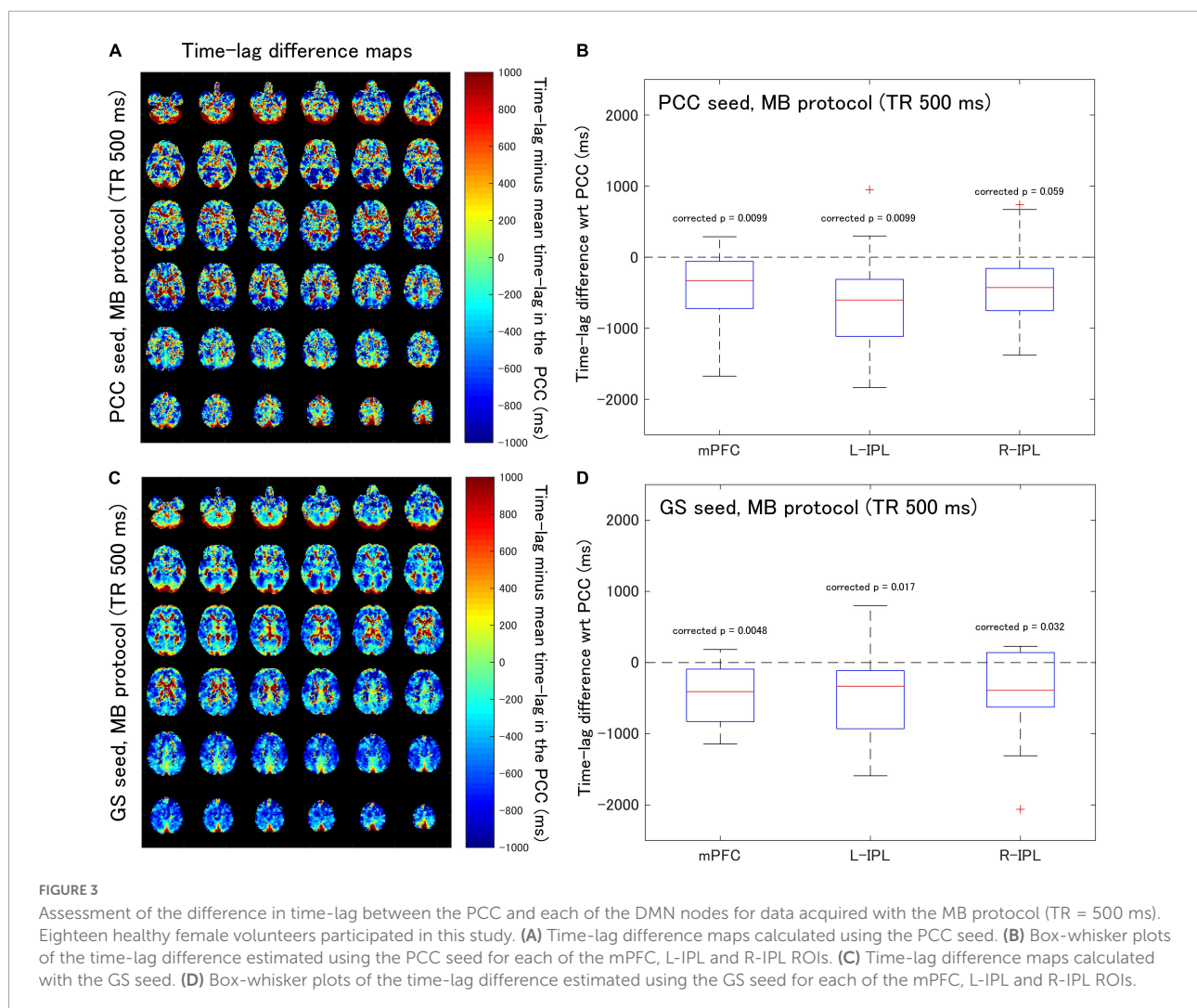
Spearman's correlation analysis was performed for the mPFC, L-IPL, and R-IPL to evaluate the relationship between the time-lag of neuronal activity, as represented by the PCC seed analysis, and the time-lag of SysLFOs, as represented by the GS seed analysis. As comparisons were performed for the three different nodes of the DMN, Bonferroni correction for multiple comparisons was applied by multiplying each  $p$ -value by 3.

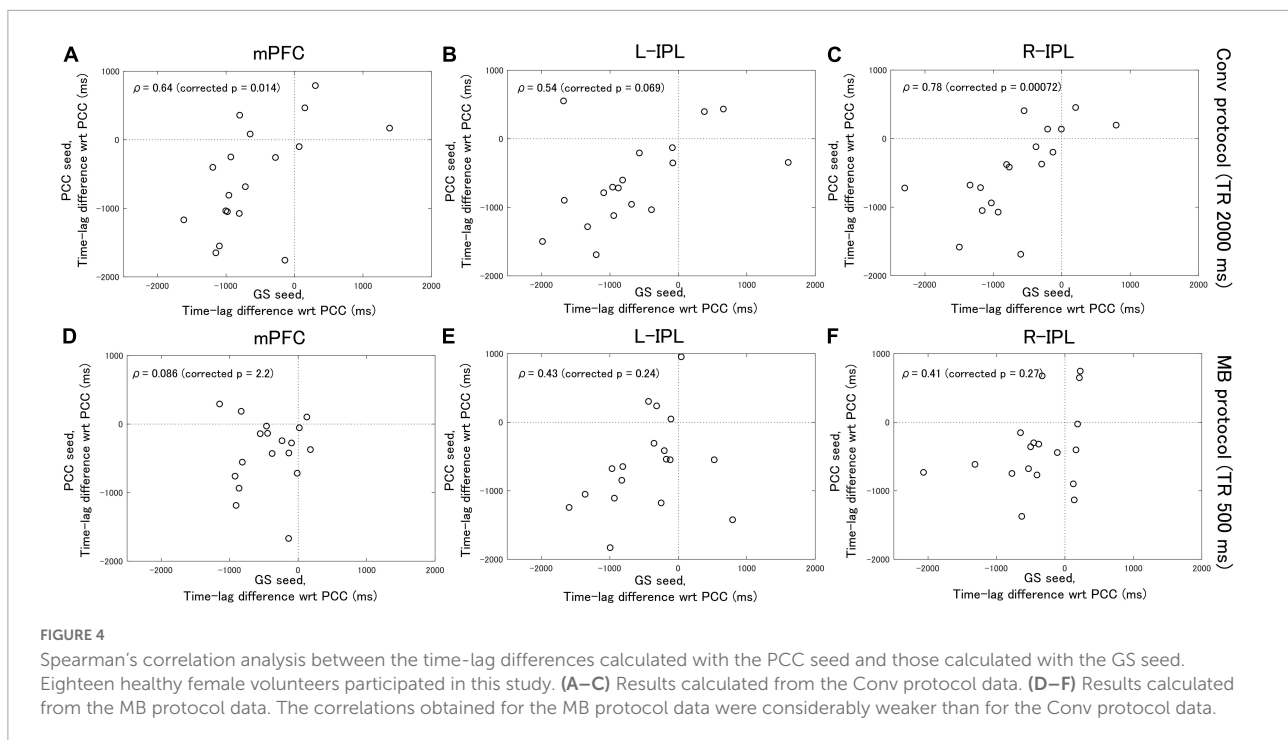
## Results

### Time-lag analysis

**Supplementary Figure 1** contains the cross-correlation curves and maps at each  $\Delta$  for one of the subjects (No. 7). Subsequently, time-lag difference maps were generated (**Figures 2A,C, 3A,C**), and time-lag analysis was performed on the Conv and MB protocol data for both the PCC and GS seeds.

For the Conv protocol data (**Figure 2**), the median time-lags estimated with the PCC seed for the mPFC, L-IPL, and R-IPL ROIs differed from the time-lag of the PCC ROI by  $-547.7$ ,  $-716.4$ , and  $-401.8$  ms, respectively (**Figure 2B**). These differences in time-lag all differed significantly from zero (mPFC, corrected  $p = 0.037$ ; L-IPL, corrected  $p = 0.0099$ ; R-IPL, corrected  $p = 0.033$ ), indicating that the responses were advanced in time compared to that of the PCC. Additionally, the median time-lags estimated using the GS seed differed from that of the PCC ROI by  $-799.1$ ,  $-841.6$ , and  $-678.7$  ms for the





mPFC, L-IPL, and R-IPL ROIs, respectively (Figure 2D). The response in each ROI was advanced in time with respect to the PCC because the differences were all significantly different from zero (mPFC, corrected  $p = 0.029$ ; L-IPL, corrected  $p = 0.022$ ; R-IPL, corrected  $p = 0.0055$ ).

When time-lag analysis was performed on the MB protocol data (Figure 3), the median time-lags estimated with the PCC seed differed from the time-lag of the PCC ROI by  $-329.3$ ,  $-602.4$ , and  $-427.8$  ms for the mPFC, L-IPL, and R-IPL ROIs, respectively (Figure 3B). The differences for the mPFC (corrected  $p = 0.0099$ ) and L-IPL (corrected  $p = 0.0099$ ) were significantly different from zero, implying a faster response in comparison to the PCC for those ROIs. However, the response in the R-IPL did not significantly differ from that of the PCC (corrected  $p = 0.059$ ). After analysing the data using the GS seed, it was found that the median time-lags of the mPFC, L-IPL, and R-IPL ROIs differed from the time-lag of the PCC ROI by  $-408.5$ ,  $-331.2$ , and  $-390.6$  ms, respectively (Figure 3D). These results were all significantly different from zero (mPFC, corrected  $p = 0.0048$ ; L-IPL, corrected  $p = 0.017$ ; R-IPL, corrected  $p = 0.032$ ), so the responses were advanced in time compared to the PCC.

## Correlation analysis

Analysis of the Conv protocol data found substantial correlations between the time-lag differences calculated with the PCC seed (see Figure 2B) and those calculated with the

GS seed (see Figure 2D). Spearman's correlation coefficient for the mPFC, L-IPL, and R-IPL was 0.64 (corrected  $p = 0.014$ , Figure 4A), 0.54 (corrected  $p = 0.069$ , Figure 4B), and 0.78 (corrected  $p = 0.00072$ , Figure 4C), respectively. In contrast, applying a similar analysis to the MB protocol data found that the correlation between the time-lag differences calculated with the PCC (see Figure 3B) and GS (see Figure 3D) seeds was much weaker. Spearman's correlation coefficient for the mPFC, L-IPL, and R-IPL was 0.086 (corrected  $p = 2.2$ , Figure 4D), 0.43 (corrected  $p = 0.24$ , Figure 4E), and 0.41 (corrected  $p = 0.27$ , Figure 4F), respectively.

## Discussion

The time-lag analysis results indicate that, even though the acquisition sampling rate of the Conv protocol is four times less than that of the MB protocol, a time-lag between nodes of the DMN was detectable with both protocols. In addition, the presence of significant time-lags between nodes indicates that the response in different nodes is highly correlated, but not simultaneous.

Based on the results of previous studies (Biswal, 2012; Erdoğan et al., 2016), in this manuscript the PCC and SysLFOs, respectively. The time-lag analysis with the PCC seed therefore provides an estimate of the delay in neuronal activity between the PCC and the other nodes of the DMN. Similarly, the time-lag analysis with the GS seed provides an estimate

of the delay between the response in different regions of the brain due to SysLFOs. Correlation analysis was then performed to compare the delays estimated with each seed. The fact that significant correlations between the delays are found for the Conv protocol data indicates that the arrival of the response due to neuronal activity cannot be distinguished from the arrival of the response due to SysLFOs. That is, functional connectivity evaluated from Conv protocol data may be heavily influenced by SysLFO signals that are of non-neuronal origin.

On the other hand, the correlation coefficients calculated from the MB protocol data suggest that the arrival of the response due to neuronal activity can be distinguished from the arrival of the response due to SysLFOs in the frequency domain 0.01–0.1 Hz. That is, the higher sampling rate of the MB protocol may allow the SysLFO contribution to the signal to be isolated. Therefore, with suitable adjustments to the analysis procedures, multiband EPI acquisition of rsfMRI data may permit resting-state neuronal activity to be studied without the obfuscating non-neuronal effects of SysLFOs.

There are a number of limitations that could have affected the results of this study. First, a relatively high multiband factor of six was employed when acquiring the MB protocol data. With such a high factor it is possible that there was signal leakage from one slice into another simultaneously excited slice (Todd et al., 2016), and this may have influenced the results of the time-lag and correlation analysis. Experiments trialing multiple multiband factors and TR protocols would be required to determine whether the leakage has a significant effect on the results. Second, even though standard motion correction, registration and normalization were applied to the data, it is impossible to guarantee that imperfect correction has not affected the results to some degree. In a similar way, although the data was bandpass filtered, it is not possible to rule out some aliasing of high frequency BOLD signal into the filtered data as noise that influences the results.

## Conclusion

In conclusion, a time-lag between nodes of the DMN was detectable with both the Conv and MB acquisition protocols, with the responses in the mPFC, L-IPL, and R-IPL being temporally advanced with respect to that in the PCC. Correlation analysis of the Conv protocol data suggested that SysLFOs substantially influence the apparent time-lag of neuronal activity. However, correlation analysis of the MB protocol data implied that the effects of SysLFOs and neuronal activity on the BOLD response may be separated. Therefore, using a higher time-resolution acquisition method for rsfMRI might help to distinguish neuronal activity induced changes to the BOLD response from those induced by SysLFOs.

## Data availability statement

The raw data supporting the conclusions of this article will be made available by the authors, without undue reservation.

## Ethics statement

The studies involving human participants were reviewed and approved by the Institutional Review Board of the National Institutes for Quantum Science and Technology (research protocol # 16-031). The patients/participants provided their written informed consent to participate in this study.

## Author contributions

All authors contributed to the conception, design, analysis, and interpretation of the data as well as to drafting the manuscript and revising it critically and read and approved the final version of the manuscript.

## Funding

This research was supported by a AMED Brain/MINDS Beyond program Grant Nos. JP22dm0307002 and JP22dm0307104.

## Conflict of interest

The authors declare that the research was conducted in the absence of any commercial or financial relationships that could be construed as a potential conflict of interest.

## Publisher's note

All claims expressed in this article are solely those of the authors and do not necessarily represent those of their affiliated organizations, or those of the publisher, the editors and the reviewers. Any product that may be evaluated in this article, or claim that may be made by its manufacturer, is not guaranteed or endorsed by the publisher.

## Supplementary material

The Supplementary Material for this article can be found online at: <https://www.frontiersin.org/articles/10.3389/fnins.2022.961686/full#supplementary-material>

## References

- Barkhof, F., Haller, S., and Rombouts, S. A. R. B. (2014). Resting-state functional MR imaging: a new window to the brain. *Radiology* 272, 29–49. doi: 10.1148/radiol.14132388
- Biswal, B. B. (2012). Resting state fMRI: a personal history. *NeuroImage* 62, 938–944. doi: 10.1016/j.neuroimage.2012.01.090
- Buxton, R. B., Uludağ, K., Dubowitz, D. J., and Liu, T. T. (2004). Modeling the hemodynamic response to brain activation. *NeuroImage* 23(Suppl. 1), S220–S233. doi: 10.1016/j.neuroimage.2004.07.013
- Chang, C., Cunningham, J. P., and Glover, G. H. (2009). Influence of heart rate on the BOLD signal: the cardiac response function. *NeuroImage* 44, 857–869. doi: 10.1016/j.neuroimage.2008.09.029
- Chang, C., and Glover, G. H. (2009). Relationship between respiration, end-tidal CO<sub>2</sub>, and BOLD signals in resting-state fMRI. *NeuroImage* 47, 1381–1393. doi: 10.1016/j.neuroimage.2009.04.048
- Erdoğan, S. B., Tong, Y., Hocke, L. M., Lindsey, K. P., and deB Frederick, B. (2016). Multiplexed echo planar imaging for sub-second whole brain functional connectivity analysis of resting state fMRI-BOLD signals. *Front. Hum. Neurosci.* 10:311. doi: 10.3389/fnhum.2016.00311
- Feinberg, D. A., Moeller, S., Smith, S. M., Auerbach, E., Ramanna, S., Gunther, M., et al. (2010). Multiplexed echo planar imaging for sub-second whole brain fmri and fast diffusion imaging. *PLoS One* 5:e0015710. doi: 10.1371/journal.pone.0015710
- Golestani, A. M., Chang, C., Kwint, J. B., Khatamian, Y. B., and Jean Chen, J. (2015). Mapping the end-tidal CO<sub>2</sub> response function in the resting-state BOLD fMRI signal: spatial specificity, test-retest reliability and effect of fMRI sampling rate. *NeuroImage* 104, 266–277. doi: 10.1016/j.neuroimage.2014.10.031
- Greicius, M. D., Krasnow, B., Reiss, A. L., and Menon, V. (2003). Functional connectivity in the resting brain: a network analysis of the default mode hypothesis. *Proc. Natl. Acad. Sci. U.S.A.* 100, 253–258. doi: 10.1073/pnas.0135058100
- Greicius, M. D., Srivastava, G., Reiss, A. L., and Menon, V. (2004). Default-mode network activity distinguishes Alzheimer's disease from healthy aging: evidence from functional MRI. *Proc. Natl. Acad. Sci. U.S.A.* 101, 4637–4642. doi: 10.1073/pnas.0308627101
- Hirano, Y., Stefanovic, B., and Silva, A. C. (2011). Spatiotemporal evolution of the functional magnetic resonance imaging response to ultrashort stimuli. *J. Neurosci.* 31, 1440–1447. doi: 10.1523/JNEUROSCI.3986-10.2011
- Hirano, Y., Yen, C. C., Liu, J. V., Mackel, J. B., Merkle, H., Nascimento, G. C., et al. (2018). Investigation of the BOLD and CBV fMRI responses to somatosensory stimulation in awake marmosets (*Callithrix jacchus*). *NMR Biomed.* 31:3864. doi: 10.1002/nbm.3864
- Julien, C. (2006). The enigma of Mayer waves: facts and models. *Cardiovasc. Res.* 70, 12–21. doi: 10.1016/j.cardiores.2005.11.008
- Liang, M., Zhou, Y., Jiang, T., Liu, Z., Tian, L., Liu, H., et al. (2006). Widespread functional disconnectivity in schizophrenia with resting-state functional magnetic resonance imaging. *NeuroReport* 17, 209–213. doi: 10.1097/01.wnr.0000198434.06518.b8
- Liu, T. T. (2013). Neurovascular factors in resting-state functional MRI. *NeuroImage* 80, 339–348. doi: 10.1016/j.neuroimage.2013.04.071
- Murphy, K., Birn, R. M., and Bandettini, P. A. (2013). Resting-state fMRI confounds and cleanup. *NeuroImage* 80, 349–359. doi: 10.1016/j.neuroimage.2013.04.001
- Nilsson, H., and Aalkjaer, C. (2003). Vasomotion: mechanisms and physiological importance. *Mol. Intervent.* 3, 79–89. doi: 10.1124/mi.3.2.79
- Obata, T., Liu, T. T., Miller, K. L., Luh, W. M., Wong, E. C., Frank, L. R., et al. (2004). Discrepancies between BOLD and flow dynamics in primary and supplementary motor areas: application of the balloon model to the interpretation of BOLD transients. *NeuroImage* 21, 144–153. doi: 10.1016/j.neuroimage.2003.08.040
- Ogawa, S., Lee, T. M., Kay, A. R., and Tank, D. W. (1990). Brain magnetic resonance imaging with contrast dependent on blood oxygenation (cerebral blood flow/brain metabolism/oxygenation). *Proc. Natl. Acad. Sci. U.S.A.* 87, 9868–9872.
- Rivadulla, C., de Labra, C., Grieve, K. L., and Cudeiro, J. (2011). Vasomotion and neurovascular coupling in the visual thalamus in vivo. *PLoS One* 6:e0028746. doi: 10.1371/journal.pone.0028746
- Sassaroli, A., Pierro, M., Bergethon, P. R., and Fantini, S. (2012). Low-frequency spontaneous oscillations of cerebral hemodynamics investigated with near-infrared spectroscopy: a review. *IEEE J. Select. Top. Quant. Electron.* 18, 1478–1492. doi: 10.1109/JSTQE.2012.2183581
- Todd, N., Moeller, S., Auerbach, E. J., Yacoub, E., Flandin, G., and Weiskopf, N. (2016). Evaluation of 2D multiband EPI imaging for high-resolution, whole-brain, task-based fMRI studies at 3T: sensitivity and slice leakage artifacts. *NeuroImage* 124, 32–42. doi: 10.1016/j.neuroimage.2015.08.056
- Tong, Y., Frederick, B. (2014). Tracking cerebral blood flow in BOLD fMRI using recursively generated regressors. *Hum. Brain Mapp.* 35, 5471–5485. doi: 10.1002/hbm.22564
- Tong, Y., Hocke, L. M., Nickerson, L. D., Licata, S. C., Lindsey, K. P., and Frederick, B. D. (2013). Evaluating the effects of systemic low frequency oscillations measured in the periphery on the independent component analysis results of resting state networks. *NeuroImage* 76, 202–215. doi: 10.1016/j.neuroimage.2013.03.019
- Tong, Y., Lindsey, K. P., Hocke, L. M., Vitaliano, G., Mintzopoulos, D., and Frederick, B. D. (2017). Perfusion information extracted from resting state functional magnetic resonance imaging. *J. Cerebr. Blood Flow Metab.* 37, 564–576. doi: 10.1177/0271678X16631755
- Wise, R. G., Ide, K., Poulin, M. J., and Tracey, I. (2004). Resting fluctuations in arterial carbon dioxide induce significant low frequency variations in BOLD signal. *NeuroImage* 21, 1652–1664. doi: 10.1016/j.neuroimage.2003.11.025